INTERNATIONAL JOURNAL OF
NUMERICAL ANALYSIS AND MODELING
Volume 13, Number 1, Pages 145–165

MONOTONICITY/SYMMETRICITY PRESERVING RATIONAL QUADRATIC FRACTAL INTERPOLATION SURFACES

ARYA KUMAR BEDABRATA CHAND AND NALLAPU VIJENDER

Abstract. This paper presents the theory of $\mathcal{C}^1$-rational quadratic fractal interpolation surfaces (FISs) over a rectangular grid. First we approximate the original function along the grid lines of interpolation domain by using the univariate $\mathcal{C}^1$-rational quadratic fractal interpolation functions (fractal boundary curves). Then we construct the rational quadratic FIS as a blending combination with the x-direction and y-direction fractal boundary curves. The developed rational quadratic FISs are monotonic whenever the corresponding fractal boundary curves are monotonic. We derive the optimal range for the scaling parameters in both positive and negative directions such that the rational quadratic fractal boundary curves are monotonic in nature. The relation between x-direction and y-direction scaling matrices is deduced for symmetric rational quadratic FISs for symmetric surface data. The presence of scaling parameters in the fractal boundary curves helps us to get a wide variety of monotonic/symmetric rational quadratic FISs without altering the given surface data. Numerical examples are provided to demonstrate the comprehensive performance of the rational quadratic FIS in fitting a monotonic/symmetric surface data. The convergence analysis of the monotonic rational quadratic FIS to the original function is reported.

Key words. Fractals, Fractal Interpolation Functions, Rational Quadratic Fractal Interpolation Surfaces, Convergence, Monotonicity, Symmetricity.

1. Introduction

The field of fractals [21] is introduced as an interdisciplinary area between branches of mathematics and physics, and later applied successfully in different areas of science and engineering. Fractals provide a powerful and effective tool to approximate projections of physical objects such as coastlines, profiles of mountains, plants as well as experimental data that have non-integer dimension. To provide an alternative tool for traditional interpolants, Barnsley [3] introduced the concept of fractal interpolation functions (FIFs) via iterated function system (IFS). A FIF contains a set of free variables called the scaling parameters. The variation of scaling parameters helps us to generate a wide variety of smooth or non-smooth FIFs for the same interpolation data. Restricting the scaling parameters with respect to the horizontal scaling parameters, Barnsley and Harrington [4] developed a method to construct a differentiable FIF that interpolates the prescribed data if the values of derivatives of an original function are known at the initial end-point of the interval. The fractal polynomial splines with general type of boundary conditions are studied recently by (i) constructive approach in [9, 14] (ii) α-fractal functions in [11, 22].

The study of fractal surfaces are useful in scientific applications such as image processing [23], geology [15], chemistry [24], etc. Geronimo and Hardin [18] developed the fractal interpolation surface on flexible domains. Simultaneously, by using barycentric co-ordinates, Zhao [26] gave two algorithms that generalize the earlier construction described in [18]. Xie and Sun [25] constructed a bivariate FIS

Received by the editors April 3, 2015.
2000 *Mathematics Subject Classification.* 28A80, 41A20, 65D05, 65D07, 65D10, 65D17, 26A48 .
The partial support of the Department of Science and Technology of Govt. of India (SERC DST Project No. SR/S4/MS: 694/10) is gratefully acknowledged.

on rectangular grids with arbitrary contraction factors and without any restriction on boundary data. Dalla [16] extemporized this construction by using collinear boundary points, and demonstrated that the attractor is a continuous FIS. Subsequent developments in this direction are carried out by Bouboulis and Dalla [6], Chand and Navascués [10], Feng et al. [17], Chand [12]. However, the constructions mentioned above may not produce the monotonic/symmetric fractal surfaces even if the given surface data is monotonic/symmetric.

Although the field of interpolation has been cultivated for centuries, the demand for more effective tools is very much active due to the modeling problems in complexity, and the manufacturing requirements in the early stage of surface design. Spline representation to visualize a scientific data is of great significance in computer graphics, geometric modeling, and numerical analysis. Although splines are smooth, they may not fulfill the user's qualitative requirements. For instance, the given data may be generated from a monotone/symmetric surface but the resulting interpolant may not satisfy these properties, and induce artificial or exaggerated hills and valleys in the interpolating surface. For the case of surface generation, several non-fractal methods have been proposed by a number of authors which preserves properties such as positivity, monotonicity and/or convexity of the data. Beatson and Ziegler [5] presented a monotonicity preserving surface interpolant over a triangular grid. This surface is uniquely determined by the functional values and first order partial derivatives at the vertices of the triangular grid. Asaturyan and Unswoth [1] developed a monotonicity preserving biquadratic splines over rectangular grids. In their approach, a modification at x-location of one edge of a sub-rectangle gives a variation throughout the grid for all sub-rectangle edges located at the original x-values, and hence the scheme is global. By developing the necessary and sufficient conditions on the first and mixed partial derivatives at grids, Carlson and Fritsch [7] produced a monotonic surface interpolant over rectangular grid. Kouibia and Pasadas [20] presented an approximation problem of parametric curves and surfaces from the Lagrange or Hermite data set. However, the shape preserving interpolation technique for the surface generation problem via fractal technique is not yet initiated. This paper specifically concentrates on the visualization of the monotonic/symmetric surface data arranged on a rectangular grid in the form of rational quadratic FISs.

In order to show the deficiency of the classical blending $\mathcal{C}^1$- cubic spline surface scheme, consider a monotonically increasing and symmetric surface data as in Table 1. For simplicity of presentation, we have used triplet $(.,.,.)$, where the first component indicates function value and second, third components represent the first order partial derivatives with respect to x-direction and y-direction, all are evaluated at the typical point (x_i, y_j). It can be easily seen that although surface data in Table 1 is increasing, the classical surface in Fig. 1 is not increasing.

TABLE 1. Monotonically increasing symmetric surface data.

$\downarrow x/y \rightarrow$	1	2	3	4
1	(1,1,1)	(2,4,2)	(3,9,3)	(4,16,4)
2	(2, 2,4)	(4, 8, 8)	(6, 18, 12)	(8,32,16)
3	(3, 3, 9)	(6, 12, 18)	(9, 27, 27)	(12, 48, 36)
4	(4, 4, 16)	(8, 16, 32)	(12, 36, 48)	(16, 64, 64)

Not only this blending surface scheme, but also several classical and fractal surface interpolation schemes do not preserve the monotonicity attached with given

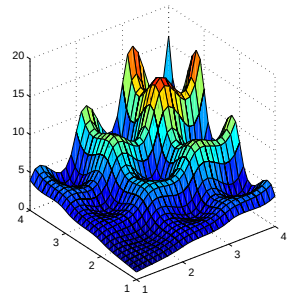

FIGURE 1. $\mathcal{C}^1$-Blending cubic spline surface.

surface data. Thus we need the surface interpolants that retain the monotonicity feature attached with surface data and that is the objective of this paper. Since rational splines are suitable for shape preserving interpolants, we have used the rational quadratic FIF in the construction of monotonicity/symmetricity preserving fractal surfaces. Our rational quadratic FIS is monotonicity preserving in the sense that if the data set exhibits monotonicity along all grid lines parallel to the axes, then the resulting rational quadratic FIS exhibits monotonicity along all lines parallel to these grid lines as well.
Important features of the proposed rational quadratic FIS are as follows:

- Our interpolant is developed in such a way that no additional knots are required to preserve the monotonicity whereas interpolant [2] needs additional knots to preserve the shape of data.
- Generated rational quadratic FISs are unique for given surface data and set of scaling parameters.
- The scaling parameters provide freedom to an user to alter the shape of monotonic/symmetric surfaces.

In Section 2, we present the basics of IFS theory and the existence of $\mathcal{C}^r$-rational FIF. In Section 3, we construct the rational quadratic fractal boundary curves in x-direction and y-direction without any restriction on the scaling parameters (except differentiability condition), then we form a $\mathcal{C}^1$-rational quadratic FIS as a combination of these fractal boundary curves and blending functions. In Section 4, simple constraints are derived on the scaling parameters so that the fractal boundary curves and resultant rational quadratic FISs are monotonic/symmetric when the given data is monotonic/symmetric, and these theoretical results are verified through numerical experiments in Section 5. The convergence result of the rational quadratic FIS to the original function is studied in Section 6.

2. Fractal Interpolation Functions

We review the basics of IFS theory in Section 2.1. The existence of $\mathcal{C}^r$-rational FIF is studied in Section 2.2.

2.1. Basics of FIF Theory. Let (X, d) be a complete metric space and $H(X)$ the class of all non-empty compact subsets of X. The set $H(X)$ is a complete metric space with respect to the Hausdorff metric h [3]. Take $(m-1)$ number of contraction maps $w_i : X \to X, i = 1, 2, \ldots, m-1$. Then $\mathcal{I} \equiv \{X; w_i, i = 1, 2, \ldots, m-1\}$ is called an iterated function system. If $w_i, i = 1, 2, \ldots, m-1$, are contractions, these maps induce a set valued function $W : H(X) \to H(X), W(E) = \cup_{i=1}^{m-1} w_i(E)$, which is a

contraction on $H(X)$ with a contraction factor $s = \max\{|s_i|; i = 1, 2, \ldots, m-1\}$, $|s_i|$ being the contraction factor of w_i. By the Banach Fixed Point theorem, there exists a unique set $A \in H(X)$ which is invariant with respect to W, that is, $A = W(A)$. The set $A \in H(X)$ is called the attractor of the IFS $\mathcal{I}$. If $\mathcal{I}$ is defined suitably, then A represents the graph of a FIF based on the following results:

Let $x_1 < x_2 < \cdots < x_{m-1} < x_m (m > 2)$ be a partition of the closed interval $I = [x_1, x_m]$, and $f_1, f_2, \ldots, f_m$ be a collection of real numbers. Let $L_i, i = 1, 2, \ldots, m-1$, be a set of homeomorphism mappings from I to $I_i = [x_i, x_{i+1}]$ satisfying

$$L_i(x_1) = x_i, L_i(x_m) = x_{i+1}. \tag{1}$$

Let $F_i(x, f)$ be a function from $I \times K$ to K (K is suitable compact sub-set of $\mathbb{R}$), which is continuous in x-direction and contractive in f-direction (with contractive factor $|\alpha_i| \leq \kappa < 1$) such that

$$F_i(x_1, f_1) = f_i, \quad F_i(x_m, f_m) = f_{i+1}, \ i = 1, 2, \ldots, m-1. \tag{2}$$

Defining a mapping $w_i : I \times K \to I_i \times K$ as $w_i(x, f) = (L_i(x), F_i(x, f)), (x, f) \in I \times K, \ i = 1, 2, \ldots, m-1$.

Proposition 2.1. *[3] For the given IFS $\{I \times K; w_i, i = 1, 2, \ldots, m-1\}$, there exists a unique compact set $A \subset \mathbb{R}^2$ such that $W(A) = A$. In addition, there is a unique continuous function g^* which satisfies $g^*(x_i) = f_i, \ i = 1, 2, \ldots, m$, and A is the graph of g^* on I. The above function ϕ is called a FIF associated with the IFS $\{I \times K; w_i, i = 1, 2, \ldots, m-1\}$.*

Now, we recall the functional equation of g^* needed for this work. Let $\mathcal{G} = \{g : I \to \mathbb{R} \mid g$ is continuous, $g(x_1) = f_1$ and $g(x_m) = f_m\}$. We define a metric on $\mathcal{G}$ by $\rho(f, g) = \max\left\{|f(x) - g(x)| \ : \ x \in I\right\}$ for $f, g \in \mathcal{G}$. Then $(\mathcal{G}, \rho)$ is a complete metric space. Define the Read-Bajraktarević operator T on $(\mathcal{G}, \rho)$ by

$$Tg(x) = F_i(L_i^{-1}(x), g \circ L_i^{-1}(x)), \ x \in I_i. \tag{3}$$

Using the properties of L_i and (1)-(2), Tg is continuous on the interval I_i ; $i = 1, 2, \ldots, m-1$, and at each of the points $x_2, \ldots, x_{m-1}$. Also it is easy to see that T is a contraction map on the complete metric space $(\mathcal{G}, \rho)$, i.e., $\rho(Tf, Tg) \leq |\alpha|_\infty \rho(f, g)$, where $|\alpha|_\infty = \max\{|\alpha_i| : i = 1, 2, \ldots, m-1\} < 1$. Therefore, by the Banach fixed point theorem, T possesses a unique fixed point (say) g^* on $\mathcal{G}$, i.e., $(Tg^*)(x) = g^*(x) \ \forall \ x \in I$. According to (3), the FIF satisfies the functional equation: $g^*(x) = F_i(L_i^{-1}(x), g^* \circ L_i^{-1}(x)), \ x \in I_i$. In the existing constructions of FIFs, $L_i(x)$ and $F_i(x, f)$ in the IFS are defined as $w_i(x, f) = \begin{bmatrix} L_i(x) \\ F_i(x, f) \end{bmatrix} = \begin{bmatrix} a_i x + b_i \\ \alpha_i f + q_i(x) \end{bmatrix}$, where $a_i = \frac{x_{i+1} - x_i}{x_m - x_1}, b_i = \frac{x_m x_i - x_1 x_{i+1}}{x_m - x_1}, |\alpha_i| \leq \kappa < 1$ and $q_i, i = 1, 2, \ldots, m-1$, are suitable continuous real valued functions defined on I such that (2) are satisfied. In the construction of the fractal boundary curves, we assume $q_i (i = 1, 2, \ldots, m-1)$ is a rational quadratic function, whose numerator and denominator are quadratic polynomials. The existence of the spline polynomial FIFs is given in [4]. Now we extend this result to rational FIF in the following.

2.2. Existence of $\mathcal{C}^r$- Rational FIF.

Theorem 2.1. *Let $\{(x_i, f_i, di) \ : \ i = 1, 2, \ldots, m\}$ be given data set, where d_i is the slope at x_i, and $d_i^{(k)}$ $(i = 1, 2, \ldots, m, k = 2, \ldots, r)$ is the k^{th} derivative value at x_i. Consider the IFS $\mathcal{I}^* \equiv \{I \times K; w_i(x, f) = (L_i(x), F_i(x, f)), i = 1, 2, \ldots, m-1\}$, where $L_i(x) = a_i x + b_i$ satisfies (1), $F_i(x, f) = \alpha_i f + q_i(x)$, $q_i(x)$ is a rational*

function on I having $2r+2$ arbitrary constants, and $|\alpha_i| < a_i^r, i = 1, 2, \ldots, m-1$. Let $F_i^k(x, f) = \frac{\alpha_i f + q_i^{(k)}(x)}{a_i^k}$, where $q_i^{(k)}(x)$ represents k^{th} derivative of $q_i(x)$ with respect to x. Denote $f_i = d_i^{(0)}, d_i = d_i^{(1)}, i = 1, 2, \ldots, m$. If for $k = 0, 1, \ldots, r$,

$$F_i^k(x_1, d_1^{(k)}) = d_i^{(k)}, F_i^k(x_m, d_m^{(k)}) = d_{i+1}^{(k)}, i = 1, 2, \ldots, m-1, \tag{4}$$

then the attractor of the IFS $\mathcal{I}^*$ is the graph of a $\mathcal{C}^r$-rational FIF.

Proof. Suppose $\mathcal{F}^r = \{g \in \mathcal{C}^r(I) \mid g(x_1) = f_1 \text{ and } g(x_m) = f_m\}$. Now $(\mathcal{F}^r, d^r)$ is a complete metric space, where d^r is the metric on $\mathcal{F}^r$ induced by the $\mathcal{C}^r$-norm on $\mathcal{C}^r(I)$. Define the Read-Bajraktarević operator U on $\mathcal{F}^r$ as

$$Ug(x) = \alpha_i g(L_i^{-1}(x)) + q_i(L_i^{-1}(x)),\ x \in I_i, i = 1, 2, \ldots, m-1. \tag{5}$$

Since $a_i = \frac{x_{i+1} - x_i}{x_m - x_1} < 1$, the conditions $|\alpha_i| < a_i^r, i = 1, 2, \ldots, m-1$, and (4) gives that U is a contractive operator on $(\mathcal{F}^r, d^r)$. The fixed point ψ of U is a fractal function that satisfies the functional equation:

$$\psi(L_i(x)) = \alpha_i \psi(x) + q_i(x), x \in I,\ i = 1, 2, \ldots, m-1. \tag{6}$$

Since $\psi \in \mathcal{C}^r(I)$, $\psi^{(k)}$ satisfies for $k = 0, 1, \ldots, r$,

$$a_i^k \psi^{(k)}(L_i(x)) = \alpha_i \psi^{(k)}(x) + q_i^{(k)}(x), x \in I, i = 1, 2, \ldots, m-1, \tag{7}$$

Using (4) in (7), we get the following system of equations for $i = 1, 2, \ldots, m-1$:

$$a_i^k d_i^{(k)} = \alpha_i d_1^{(k)} + q_i^{(k)}(x_1), \quad a_i^k d_{i+1}^{(k)} = \alpha_i d_m^{(k)} + q_i^{(k)}(x_m)\ \forall\ k = 0, 1, \ldots, r. \tag{8}$$

When all the $2r+2$ arbitrary constants in $q_i(x)$ are determined from (8), $\psi(x)$ exists. By using the similar arguments as in [3], it is easy to conclude that IFS $\mathcal{I}^*$ has a unique attractor, and it is the graph of the rational FIF $\psi \in \mathcal{C}^r(I)$. □

3. Rational Quadratic Fractal Interpolation Surfaces

In Section 3.1, we construct the fractal boundary curves by using Theorem 2.1. Then using these fractal boundary curves, the $\mathcal{C}^1$-rational quadratic FIS is constructed in Section 3.2.

3.1. Construction of $\mathcal{C}^1$-Fractal Boundary Curves. Let $x_1 < x_2 < \cdots < x_{m-1} < x_m$, $y_1 < y_2 < \cdots < y_{n-1} < y_n$, be a partition of $D = I \times J$, $I = [x_1, x_m]$, $J = [y_1, y_n]$. Set $I_i = [x_i, x_{i+1}]$, $J_j = [y_j, y_{j+1}]$, and $D_{i,j} = I_i \times J_j, i = 1, 2, \ldots, m-1$, $j = 1, 2, \ldots, n-1$. Consider the interpolation data as $\{(x_i, y_j, z_{i,j}, z_{i,j}^x, z_{i,j}^y) : i = 1, 2, \ldots, m, j = 1, 2, \ldots, n\}$ on the rectangular D, where $z_{i,j}^x, z_{i,j}^y$ respectively are the first order partial derivatives of the original function with respect to the variables x, y at (x_i, y_j). Note that for $j = 1, 2, \ldots, n$, $T_j = \{(x_i, z_{i,j}, z_{i,j}^x) : i = 1, 2, \ldots, m\}$ is the interpolation data along the j^{th} grid line parallel to the x-axis. Similarly, for $i = 1, 2, \ldots, m$, $T_i^* = \{(y_j, z_{i,j}, z_{i,j}^y) : j = 1, 2, \ldots, n\}$ is the interpolation data along the i^{th} grid line parallel to the y-axis.

Based on Theorem 2.1, consider the following fractal boundary curve B_j along the grid line $I \times y_j$ for fixed $j \in \{1, 2, \ldots, n\}$:

$$B_j(x) = \begin{cases} \alpha_{i,j} B_j(L_i^{-1}(x)) + \frac{X_{i,j}\theta^2 + Y_{i,j}\theta(1-\theta) + Z_{i,j}(1-\theta)^2}{\triangle_{i,j}\theta^2 + W_{i,j}\theta(1-\theta) + \triangle_{i,j}(1-\theta)^2}, & \text{if } \triangle_{i,j} \neq 0, \\ z_{i,j}, & \text{if } \triangle_{i,j} = 0, \end{cases} \tag{9}$$

where $\theta = \frac{L_i^{-1}(x)-x_1}{x_m-x_1}, x \in I_i$, $\triangle_{i,j} = \frac{z_{i+1,j}-z_{i,j}}{x_{i+1}-x_i}$, $|\alpha_{i,j}| < a_i < 1, i = 1, 2, \ldots, m-1, j = 1, 2, \ldots, n$. $W_{i,j}, X_{i,j}, Y_{i,j}, Z_{i,j}$ are arbitrary constants that are evaluated respectively using the Hermite interpolation conditions:

$$B_j(x_i) = z_{i,j}, B_j(x_{i+1}) = z_{i+1,j}, B_j'(x_i) = z_{i,j}^x, B_j'(x_{i+1}) = z_{i+1,j}^x.$$

Taking $x = x_i$ in (9), we have

$$B_j(x_i) = \alpha_{i,j}B_j(x_1) + \frac{Z_{i,j}}{\triangle_{i,j}} \Rightarrow Z_{i,j} = \triangle_{i,j}(z_{i,j} - \alpha_{i,j}z_{1,j}).$$

Similarly for $x = x_{i+1}$ in (9), we obtain $X_{i,j} = \triangle_{i,j}(z_{i+1,j} - \alpha_{i,j}z_{m,j})$. Using $B_j'(x_i) = z_{i,j}^x$, $B_j'(x_{i+1}) = z_{i+1,j}^x$ in (9), we have the coupled equations:

$$\begin{cases} \triangle_{i,j}Y_{i,j} - Z_{i,j}W_{i,j} - \triangle_{i,j}^2(x_m - x_1)(a_i z_{i,j}^x - \alpha_{i,j}z_{1,j}^x) = 0, \\ X_{i,j}W_{i,j} - \triangle_{i,j}Y_{i,j} - \triangle_{i,j}^2(x_m - x_1)(a_i z_{i+1,j}^x - \alpha_{i,j}z_{m,j}^x) = 0. \end{cases} \tag{10}$$

Since $\alpha_{i,j}$ can be chosen as $|\alpha_{i,j}| < a_i < 1$, assume that $z_{i+1,j} - z_{i,j} - \alpha_{i,j}(z_{m,j} - z_{1,j}) \neq 0$. The solution of the system (10) gives that

$$W_{i,j} = \beta_{i,j}\{a_i(z_{i,j}^x + z_{i+1,j}^x) - \alpha_{i,j}(z_{1,j}^x + z_{m,j}^x)\},$$

$$\begin{aligned} Y_{i,j} =& \beta_{i,j}\{(z_{i,j}z_{i+1,j}^x + z_{i+1,j}z_{i,j}^x)a_i - \alpha_{i,j}(z_{i+1,j}z_{1,j}^x + z_{i,j}z_{m,j}^x + z_{m,j}z_{i,j}^x a_i \\ &+ z_{1,j}z_{i+1,j}^x a_i) + \alpha_{i,j}^2(z_{m,j}z_{1,j}^x + z_{1,j}z_{m,j}^x\}, \end{aligned}$$

where $\beta_{i,j} = \dfrac{\triangle_{i,j}(x_m - x_1)}{z_{i+1,j} - z_{i,j} - \alpha_{i,j}(z_{m,j} - z_{1,j})}$. By substituting the values of $W_{i,j}, X_{i,j}$, $Y_{i,j}$, $Z_{i,j}$ in (9), we get the fractal boundary curve B_j interpolating the data set T_j for $j = 1, 2, \ldots, n$, as

$$B_j(x) = \begin{cases} \alpha_{i,j}B_j(L_i^{-1}(x)) + \frac{p_{i,j}(\theta)}{q_{i,j}(\theta)}, & \text{if } \triangle_{i,j} \neq 0, \\ z_{i,j}, & \text{if } \triangle_{i,j} = 0, \end{cases} \tag{11}$$

$$\begin{aligned} p_{i,j}(\theta) =& (z_{i+1,j} - \alpha_{i,j}z_{m,j})\triangle_{i,j}\theta^2 + \beta_{i,j}\{(z_{i,j}z_{i+1,j}^x + z_{i+1,j}z_{i,j}^x)a_i - \alpha_{i,j}[z_{i+1,j}z_{1,j}^x \\ &+ z_{i,j}z_{m,j}^x + a_i(z_{m,j}z_{i,j}^x + z_{1,j}z_{i+1,j}^x)] + \alpha_{i,j}^2(z_{m,j}z_{1,j}^x + z_{1,j}z_{m,j}^x)\}\theta(1-\theta) \\ &+ (z_{i,j} - \alpha_{i,j}z_{1,j})\triangle_{i,j}(1-\theta)^2, \\ q_{i,j}(\theta) =& \triangle_{i,j}\theta^2 + \beta_{i,j}\{a_i(z_{i,j}^x + z_{i+1,j}^x) - \alpha_{i,j}(z_{1,j}^x + z_{m,j}^x)\}\theta(1-\theta) + \triangle_{i,j}(1-\theta)^2. \end{aligned}$$

Thus we have exactly n different fractal boundary curves in x-direction such that their graphs are attractors of the IFSs for $j = 1, 2, \ldots, n$,

$$\mathcal{I}_j \equiv \Big\{I \times K_{x,j} : w_{i,j}(x, z) = (L_i(x), F_{i,j}(x, z)), i = 1, 2, \ldots, m-1\Big\}, \tag{12}$$

$$\text{where } F_{i,j}(x, z) = \begin{cases} \alpha_{i,j}z + \dfrac{p_{i,j}(\theta)}{q_{i,j}(\theta)}, & \text{if } \triangle_{i,j} \neq 0, \\ z_{i,j}, & \text{if } \triangle_{i,j} = 0, \end{cases}$$

$p_{i,j}, q_{i,j}$ are given in (11), and $K_{x,j}$ are suitable compact subsets of $\mathbb{R}$. The scaling parameters $\alpha_{i,j}, i = 1, 2, \ldots, m-1, j = 1, 2, \ldots, n$, involved in the IFSs $\mathcal{I}_j, j = 1, 2, \ldots, n$, are arranged in the matrix form as $\alpha = [\alpha_{i,j}]_{(m-1)\times n}$.

Using similar arguments as above, we obtain the fractal boundary curve B_i^* interpolating the data set T_i^* for $i = 1, 2, \ldots, m$, as

$$B_i^*(y) = \begin{cases} \alpha_{i,j}^* B_i^*(L_j^{*-1}(y)) + \frac{p_{i,j}^*(\phi)}{q_{i,j}^*(\phi)}, & \text{if } \triangle_{i,j}^* \neq 0, \\ z_{i,j}, & \text{if } \triangle_{i,j}^* = 0, \end{cases} \tag{13}$$

$$\begin{aligned}p^*_{i,j}(\phi) =&(z_{i,j+1} - \alpha^*_{i,j} z_{i,n})\triangle^*_{i,j}\phi^2 + \beta^*_{i,j}\{(z_{i,j}z^y_{i,j+1} + z_{i,j+1}z^y_{i,j})c_j - \alpha^*_{i,j}[z_{i,j+1}z^y_{i,1}\\ &+ z_{i,j}z^y_{i,n} + c_j(z_{i,n}z^y_{i,j} + z_{i,1}z^y_{i,j+1})] + \alpha^{*2}_{i,j}(z_{i,n}z^y_{i,1} + z_{i,1}z^y_{i,n})\}\phi(1-\phi)\\ &+ (z_{i,j} - \alpha^*_{i,j}z_{i,1})\triangle^*_{i,j}(1-\phi)^2,\\ q^*_{i,j}(\phi) =&\triangle^*_{i,j}\phi^2 + \beta^*_{i,j}\{c_j(z^y_{i,j} + z^y_{i,j+1}) - \alpha^*_{i,j}(z^y_{i,1} + z^y_{i,n})\}\phi(1-\phi) + \triangle^*_{i,j}(1-\phi)^2,\end{aligned}$$

$\triangle^*_{i,j} = \frac{z_{i,j+1}-z_{i,j}}{y_{j+1}-y_j}, \beta^*_{i,j} = \dfrac{\triangle^*_{i,j}(y_n - y_1)}{z_{i,j+1} - z_{i,j} - \alpha^*_{i,j}(z_{i,n} - z_{i,1})}, \phi = \frac{L^{*-1}_j(y)-y_1}{y_n-y_1}$, $y \in J_j$, $h^*_j = y_{j+1} - y_j$, $\alpha^*_{i,j}$ is the scaling parameter in y-direction satisfying $|\alpha^*_{i,j}| < c_j, L^*_j(y) = c_j y + d_j : J \to J_j$ is a linear homeomorphism such that $L^*_j(y_1) = y_j, L^*_j(y_n) = y_{j+1}, j = 1, 2, \ldots, n-1$.

From (13), it is seen that exactly m different y-direction fractal boundary curves are possible such that their graphs are attractors of the IFSs for $i = 1, 2, \ldots, m$,

$$\mathcal{I}^*_i \equiv \Big\{J \times K_{y,i} : w^*_{i,j}(y, z^*) = (L^*_j(y), F^*_{i,j}(y, z^*)), j = 1, 2, \ldots, n-1\Big\}, \tag{14}$$

$$\text{where } F^*_{i,j}(y, z^*) = \begin{cases} \alpha^*_{i,j} z^* + \frac{p^*_{i,j}(\phi)}{q^*_{i,j}(\phi)}, & \text{if } \triangle^*_{i,j} \neq 0,\\ z_{i,j}, & \text{if } \triangle^*_{i,j} = 0,\end{cases}$$

$p^*_{i,j}, q^*_{i,j}$ are given in (13), and $K_{y,i}$ are suitable compact subsets of $\mathbb{R}$. The scaling parameters $\alpha^*_{i,j}, i = 1, 2, \ldots, m, j = 1, 2, \ldots, n-1$, involved in the IFSs $\mathcal{I}^*_i, i = 1, 2, \ldots, m$, are arranged in the matrix form as $\alpha^* = [\alpha^*_{i,j}]_{m\times(n-1)}$.

3.2. Formation of $\mathcal{C}^1$-Rational Quadratic Fractal Interpolation Surface. The boundary of sub-rectangle $D_{i,j}$ is taken as the union of four straight lines $I_i \times y_j, I_i \times y_{j+1}, x_i \times J_j$, and $x_{i+1} \times J_j$. Now we construct a fractal function $\Psi : D \to \mathbb{R}$ so that Ψ and its first order partial derivatives coincide with fractal boundary curves and the derivatives of fractal boundary curves along the grid lines of the rectangular domain respectively. In other words,

$$\begin{cases} \Psi\,|_{I\times y_j} = B_j, j = 1, 2, \ldots, n,\ \Psi\,|_{x_i\times J} = B^*_i, i = 1, 2, \ldots, m,\\ \dfrac{\partial\Psi}{\partial x}\,|_{I\times y_j} = B^{(1)}_j,\ j = 1, 2, \ldots, n,\ \dfrac{\partial\Psi}{\partial y}\,|_{x_i\times J} = B^{*(1)}_i,\ i = 1, 2, \ldots, m.\end{cases} \tag{15}$$

Now the fractal boundary curves (11) and (13) are used to define fractal function Ψ over each sub-rectangular domain $D_{i,j}$, $i = 1, 2, \ldots, m-1$, $j = 1, 2, \ldots, n-1$, as

$$\begin{cases}\Psi(x, y) =&b_{y,0}(\phi)B_j(x) + b_{y,1}(\phi)B_{j+1}(x) + a_{x,0}(\theta)B^*_i(y)\\ &+ a_{x,1}(\theta)B^*_{i+1}(y) - a_{x,0}(\theta)b_{y,0}(\phi)z_{i,j} - a_{x,0}(\theta)b_{y,1}(\phi)z_{i,j+1}\\ &- a_{x,1}(\theta)b_{y,0}(\phi)z_{i+1,j} - a_{x,1}(\theta)b_{y,1}(\phi)z_{i+1,j+1},\end{cases} \tag{16}$$

The functions $a_{x,0}, a_{x,1}, b_{y,0}$, and $b_{y,1}$ are differentiable functions on $[0, 1]$. By applying (15) in (16), we get the following conditions on the functions $a_{x,0}$, $a_{x,1}$, $b_{y,0}$, and $b_{y,1}$:

$$\begin{cases} a_{x,0}(0) = 1,\ a_{x,1}(0) = 0,\ a_{x,0}(1) = 0,\ a_{x,1}(1) = 1,\\ a^{(1)}_{x,0}(0) = 0,\ a^{(1)}_{x,1}(0) = 0,\ a^{(1)}_{x,0}(1) = 0,\ a^{(1)}_{x,1}(1) = 0,\\ b_{y,0}(0) = 1,\ b_{y,1}(0) = 0,\ b_{y,0}(1) = 0,\ b_{y,1}(1) = 1,\\ b^{(1)}_{y,0}(0) = 0,\ b^{(1)}_{y,1}(0) = 0,\ b^{(1)}_{y,0}(1) = 0,\ b^{(1)}_{y,1}(1) = 0.\end{cases} \tag{17}$$

For simplicity, we take each function $a_{x,0}(\theta)$, $a_{x,1}(\theta)$, $b_{y,0}(\phi)$, and $b_{y,1}(\phi)$ as cubic polynomial containing four arbitrary constants. After evaluation of arbitrary constants in the polynomials using conditions in (17), the functions $a_{x,0}$, $a_{x,1}$, $b_{y,0}$, and

$b_{y,1}$ take the following form:

$$a_{x,0}(\theta) = (1-\theta)^2(1+2\theta),\ a_{x,1}(\theta) = \theta^2(3-2\theta),$$
$$b_{y,0}(\phi) = (1-\phi)^2(1+2\phi),\ b_{y,1}(\phi) = \phi^2(3-2\phi).$$

We refer the functions $a_{x,0}, a_{x,1}, b_{y,0}$, and $b_{y,1}$ as blending functions. Since we have used only rational quadratic FIFs in the construction of Ψ, we refer to it as rational quadratic FIS. Since the FIS Ψ is sum of continuous functions, it is continuous inside $D_{i,j}$, $i = 1, 2, \ldots, m-1$, $j = 1, 2, \ldots, n-1$. Next, using (16), the fractal surface Ψ can be defined over the sub-rectangle $D_{i,j+1}$ as blending of affine FIFs $B_{j+1}(x)$, $B_{j+2}(x)$, $x \in I_i$, $B_i^*(y)$, $B_{i+1}^*(y)$, $y \in J_{j+1}$. Furthermore, Ψ is continuous over $D_{i,j+1}$. Now using (17), it is verified that

$$\lim_{\substack{(x,y)\to(x,y_{j+1})\\(x,y)\in D_{i,j+1}}} \Psi(x,y) = B_{j+1}(x) = \lim_{\substack{(x,y)\to(x,y_{j+1})\\(x,y)\in D_{i,j}}} \Psi(x,y).$$

Hence Ψ is continuous on the domains $D_{i,j} \cap D_{i,j+1}$, $i = 1, 2, \ldots, m-1$, $j = 1, 2, \ldots, n-2$. Similarly we can show that Ψ is continuous on the domains $D_{i,j} \cap D_{i+1,j}$, $i = 1, 2, \ldots, m-2$, $j = 1, 2, \ldots, n-1$. From the above discussion, we conclude that the fractal surface Ψ is continuous over the interpolation domain D. In the similar way, we can observe that $\frac{\partial \Psi(x,y)}{\partial x}$ and $\frac{\partial \Psi(x,y)}{\partial y}$ are continuous in the domain D. Since the both first order partial derivatives of the rational quadratic FIS Ψ are continuous, $\Psi^{(1)}$ exists, and is continuous over the domain D. Thus the rational quadratic FIS $\Psi \in \mathcal{C}^1(D)$.

Remark 3.1. *If $\alpha = [0]_{(m-1)\times n}$ and $\alpha^* = [0]_{m\times(n-1)}$, then we get the classical rational quadratic surface interpolant as*

$$\begin{aligned} S(x,y) =& b_{y,0}(\phi)S_j(x) + b_{y,1}(\phi)S_{j+1}(x) + a_{x,0}(\theta)S_i^*(y) + a_{x,1}(\theta)S_{i+1}^*(y) \\ &- a_{x,0}(\theta)\cdot b_{y,0}(\phi)z_{i,j} - a_{x,0}(\theta)b_{y,1}(\phi)z_{i,j+1} \\ &- a_{x,1}(\theta)b_{y,0}(\phi)z_{i+1,j} - a_{x,1}(\theta)b_{y,1}(\phi)z_{i+1,j+1}, \end{aligned} \tag{18}$$

where S_j, $j = 1, 2, \ldots, n$ and S_i^*, $i = 1, 2, \ldots, m$ are the classical rational quadratic interpolants [19] obtained by taking $\alpha = [0]_{(m-1)\times n}$ and $\alpha^* = [0]_{m\times(n-1)}$ in B_j, $j = 1, 2, \ldots, n$ and B_i^*, $i = 1, 2, \ldots, m$ respectively.

4. Monotonic/Symmetric Fractal Surface Interpolation

The theory of monotonic rational quadratic FIS is given in Section 4.1. Symmetricity preserving surface interpolation via rational quadratic FIS is discussed in Section 4.2.

4.1. Theory of Monotonic FIS. For the given interpolation surface data, the shape of the interpolation surface is fixed in the classical methods due to the uniqueness of the interpolant. But the presence of the scaling parameters in the IFSs $\mathcal{I}_j, j = 1, 2, \ldots, n$, and $\mathcal{I}_i^*, i = 1, 2, \ldots, m$, gives a flexibility in the choice of fractal boundary curves by changing the corresponding scaling parameters. Thus, the shape of the rational quadratic FIS (cf. (16)) can be modified by changing the associated fractal boundary curves appropriately. However, for the scaling parameters $\alpha_{i,j} \in (-a_i, a_i)$, $i = 1, 2, \ldots, m-1$, and $\alpha_{i,j}^* \in (-c_j, c_j)$, $j = 1, 2, \ldots, n-1$, the $\mathcal{C}^1$-fractal boundary curves B_j and B_i^* need not be monotonic even if data sets T_j and T_i^* are monotonic respectively. In this section, we deduce the optimal range for the IFS parameters such that the fractal boundary curves B_j, $j = 1, 2, \ldots, n$, and B^*, $i = 1, 2, \ldots, m$, are $\mathcal{C}^1$- smooth and monotonic on I and J respectively. Using these monotonic fractal boundary curves with the blending functions, we construct

the monotonic rational quadratic FISs over the rectangle D. The following theorem addresses the desired range for the scaling parameters for a monotonic rational quadratic FIS for given monotonic surface data.

Theorem 4.1. *Let* $\{(x_i, y_j, z_{i,j}, z^x_{i,j}, z^y_{i,j}) : i = 1, 2, \ldots, m, j = 1, 2, \ldots, n\}$ *be a monotonic data set, i.e., monotonic in x-direction :* $z_{i,j} \le z_{i+1,j} (z_{i,j} \ge z_{i+1,j}), i = 1, 2, \ldots, m-1, j = 1, 2, \ldots, n$, *monotonic in y-direction :* $z_{i,j} \le z_{i,j+1} (z_{i,j} \ge z_{i,j+1}), i = 1, 2, \ldots, m, j = 1, 2, \ldots, n-1$, *with necessary conditions:* $z^x_{i,j} \ge 0$ $(z^x_{i,j} \le 0)$, $z^y_{i,j} \ge 0$ $(z^y_{i,j} \le 0), i = 1, 2, \ldots, m, j = 1, 2, \ldots, n$. *If (i) the scaling parameters* $\alpha_{i,j}, i = 1, 2, \ldots, m-1, j = 1, 2, \ldots, n$, *are chosen as*

$$\alpha_{i,j} \in (\lambda^*_{x,i,j}, \lambda_{x,i,j}), \text{ where} \tag{19}$$

$$\lambda_{x,i,j} = \min\Big\{\frac{a_i(z^x_{i+1,j} - k_{x,1,j})}{z^x_{m,j} - k_{x,1,j}}, \frac{a_i(z^x_{i,j} - k_{x,1,j})}{z^x_{1,j} - k_{x,1,j}}, \frac{a_i(k_{x,2,j} - z^x_{i+1,j})}{k_{x,2,j} - z^x_{m,j}}, \frac{a_i(k_{x,2,j} - z^x_{i,j})}{k_{x,2,j} - z^x_{1,j}},$$
$$\frac{h_i(\triangle_{i,j} - k_{x,1,j})}{z_{m,j} - z_{1,j} - k_{x,1,j}}, \frac{h_i(k_{x,2,j} - \triangle_{i,j})}{k_{x,2,j} - (z_{m,j} - z_{1,j})}, a_i\Big\},$$

$$\lambda^*_{x,i,j} = \max\Big\{\frac{-a_i(z^x_{i+1,j} - k_{x,1,j})}{k_{x,2,j} - z^x_{m,j}}, \frac{-a_i(z^x_{i,j} - k_{x,1,j})}{k_{x,2,j} - z^x_{1,j}}, \frac{-a_i(k_{x,2,j} - z^x_{i+1,j})}{z^x_{m,j} - k_{x,1,j}},$$
$$\frac{-a_i(k_{x,2,j} - z^x_{i,j})}{z^x_{1,j} - k_{x,1,j}}, \frac{-h_i(\triangle_{i,j} - k_{x,1,j})}{k_{x,2,j} - (z_{m,j} - z_{1,j})}, \frac{-h_i(k_{x,2,j} - \triangle_{i,j})}{z_{m,j} - z_{1,j} - k_{x,1,j}}, -a_i\Big\},$$

$$0 \le k_{x,1,j} < \min\{z^x_{1,j}, z^x_{i+1,j}, z_{m,j} - z_{1,j}, \triangle_{i,j};\ i = 1, 2, \ldots, m-1\},$$

$$k_{x,2,j} > \max\{z^x_{1,j}, z^x_{i+1,j}, z_{m,j} - z_{1,j}, \triangle_{i,j};\ i = 1, 2, \ldots, m-1\},$$

(ii) the scaling parameters $\alpha^*_{i,j}, i = 1, 2, \ldots, m, j = 1, 2, \ldots, n-1$, *are selected as*

$$\alpha^*_{i,j} \in (\lambda^*_{y,i,j}, \lambda_{y,i,j}), \text{ where} \tag{20}$$

$$\lambda_{y,i,j} = \min\Big\{\frac{c_j(z^y_{i,j+1} - k_{y,1,i})}{z^y_{i,n} - k_{y,1,i}}, \frac{c_j(z^y_{i,j} - k_{y,1,i})}{z^y_{i,1} - k_{y,1,i}}, \frac{c_j(k_{y,2,i} - z^y_{i,j+1})}{k_{y,2,i} - z^y_{i,n}}, \frac{c_j(k_{y,2,i} - z^y_{i,j})}{k_{y,2,i} - z^y_{i,1}},$$
$$\frac{h^*_j(\triangle^*_{i,j} - k_{y,1,i})}{z_{i,n} - z_{i,1} - k_{y,1,i}}, \frac{h^*_j(k_{y,2,i} - \triangle^*_{i,j})}{k_{y,2,i} - (z_{i,n} - z_{i,1})}, c_j\},$$

$$\lambda^*_{y,i,j} = \max\Big\{\frac{-c_j(z^y_{i,j+1} - k_{y,1,i})}{k_{y,2,i} - z^y_{i,n}}, \frac{-c_j(z^y_{i,j} - k_{y,1,i})}{k_{y,2,i} - z^y_{i,1}}, \frac{-c_j(k_{y,2,i} - z^y_{i,j+1})}{z^y_{i,n} - k_{y,1,i}},$$
$$\frac{-c_j(k_{y,2,i} - z^y_{i,j})}{z^y_{i,1} - k_{y,1,i}}, \frac{-h^*_j(\triangle^*_{i,j} - k_{y,1,i})}{k_{y,2,i} - (z_{i,n} - z_{i,1})}, \frac{-h^*_j(k_{y,2,i} - \triangle^*_{i,j})}{z_{i,n} - z_{i,1} - k_{y,1,i}}, -c_j\},$$

$$0 \le k_{y,1,i} < \min\{z^y_{i,1}, z^y_{i,j+1}, z_{i,n} - z_{i,1}, \triangle^*_{i,j};\ j = 1, 2, \ldots, n-1\},$$

$$k_{y,2,i} > \max\{z^y_{i,1}, z^y_{i,j+1}, z_{i,n} - z_{i,1}, \triangle^*_{i,j};\ j = 1, 2, \ldots, n-1\},$$

then the fractal boundary curves described in (11) and (13) are monotonic over I *and* J *respectively, and consequently the rational quadratic FIS* Ψ *(cf. 16) is monotonic over the domain* D.

Proof. Without loss of generality, assume that the given surface data is monotonically increasing. For $j = 1, 2, \ldots, n$, the fractal boundary curve B_j is monotonically increasing over I if $B'_j(x) \ge 0$ for all $x \in I$. After some algebraic manipulation, we observe that the graph of $B'_j(x)$, $x \in I$ is the attractor of the IFS

$$\mathcal{I}^d_j \equiv \Big\{I \times K^d_{x,j}; w^d_{i,j}(x, z^d) = (L_i(x), F^d_{i,j}(x, z^d)), i = 1, 2, \ldots, m-1\Big\}, \tag{21}$$

where

$$
\begin{aligned}
F^d_{i,j}(x,z^d) &= \frac{\alpha_{i,j}}{a_i}z^d + \frac{\Omega_{1,i,j}(x)}{a_i\Omega_{2,i,j}(x)},\\
\Omega_{1,i,j}(x) &= T_{i,j,1}\theta^4 + T_{i,j,2}\theta^3(1-\theta) + T_{i,j,3}\theta^2(1-\theta)^2\\
&\quad + T_{i,j,4}\theta(1-\theta)^3 + T_{i,j,5}(1-\theta)^4,\\
T_{i,j,1} &= a_i z^x_{i+1,j} - \alpha_{i,j}z^x_{m,j},\\
T_{i,j,2} &= 2a_i(\tau_{i,j}\triangle_{i,j} - z^x_{i,j}) - 2\alpha_{i,j}[\frac{\tau_{i,j}(z_{m,j}-z_{1,j})}{x_m - x_1} - z^x_{1,j}],\\
T_{i,j,3} &= a_i\big((\tau^2_{i,j}+3)\triangle_{i,j} - \tau_{i,j}(z^x_{i,j}+z^x_{i+1,j})\big)\\
&\quad - \alpha_{i,j}\Big[\frac{(\tau^2_{i,j}+3)(z_{m,j}-z_{1,j})}{x_m-x_1} - \tau_{i,j}(z^x_{1,j}+z^x_{m,j})\Big],\\
T_{i,j,4} &= 2a_i(\tau_{i,j}\triangle_{i,j} - z^x_{i+1,j}) - 2\alpha_{i,j}\big[\frac{\tau_{i,j}(z_{m,j}-z_{1,j})}{x_m-x_1} - z^x_{m,j}\big],\\
T_{i,j,5} &= a_i z^x_{i,j} - \alpha_{i,j}z^x_{1,j}, \tau_{i,j} = 1 + \frac{h_i(z^x_{i,j}+z^x_{i+1,j}) - \alpha_{i,j}(x_m-x_1)(z^x_{1,j}+z^x_{m,j})}{z_{i+1,j}-z_{i,j}-\alpha_{i,j}(z_{m,j}-z_{1,j})},\\
\Omega_{2,i,j}(x) &= 1 + (\tau_{i,j}-3)^2\theta^2(1-\theta)^2 + 2(\tau_{i,j}-3)\theta(1-\theta),
\end{aligned}
$$

and $K^d_{x,j}$ is a suitable compact subset of $\mathbb{R}$. Since the graph of $B'_j(x)$ is the attractor of the IFS $\mathcal{I}^d_j$, it is easy to verify that $B'_j(x) \geq 0$ for all $x \in I$, if

$$F^d_{i,j}(x,z^d) \in [k_{x,1,j}, k_{x,2,j}]\ \forall (x,z^d) \in I \times [k_{x,1,j}, k_{x,2,j}], i = 1,2,\ldots,m-1.$$

Next we derive the optimal range for the scaling parameters $\alpha_{i,j}, i = 1,2,\ldots, m-1, j = 1,2,\ldots,n$, such that the range of $F^d_{i,j}$ is contained in $[k_{x,1,j}, k_{x,2,j}]$.
Case-I For differentiability of $B_j(x)$, we have $0 \leq \alpha_{i,j} < a_i, i = 1,2,\ldots, m-1$, $j = 1,2,\ldots,n$. Assume that $k_{x,1,j} \leq z^d \leq k_{x,2,j}, j = 1,2,\ldots,n$. From these inequalities, we have

$$\frac{k_{x,1,j}\alpha_{i,j}}{a_i} \leq \frac{z^d\alpha_{i,j}}{a_i} \leq \frac{\alpha_{i,j}k_{x,2,j}}{a_i}, \text{ and hence}$$

$$\frac{k_{x,1,j}\alpha_{i,j}}{a_i} + \frac{\Omega_{1,i,j}(x)}{a_i\Omega_{2,i,j}(x)} \leq \frac{z^d\alpha_{i,j}}{a_i} + \frac{\Omega_{1,i,j}(x)}{a_i\Omega_{2,i,j}(x)} \leq \frac{\alpha_{i,j}k_{x,2,j}}{a_i} + \frac{\Omega_{1,i,j}(x)}{a_i\Omega_{2,i,j}(x)}. \tag{22}$$

From (22), it is easy to see that $F^d_{i,j}(x,z^d) \in [k_{x,1,j}, k_{x,2,j}]$ for every $(x,z^d) \in I \times [k_{x,1,j}, k_{x,2,j}]$, $i = 1,2,\ldots,m-1$, $j = 1,2,\ldots,n$, if

- $\Pi_{1,i,j}(x) := \frac{k_{x,1,j}[\alpha_{i,j}-a_i]}{a_i} + \frac{\Omega_{1,i,j}(x)}{a_i\Omega_{2,i,j}(x)} \geq 0,$
- $\Pi_{2,i,j}(x) := \frac{k_{x,2,j}[\alpha_{i,j}-a_i]}{a_i} + \frac{\Omega_{1,i,j}(x)}{a_i\Omega_{2,i,j}(x)} \leq 0.$

After some simplification, $\Pi_{1,i,j}(x)$ is re-written as

$$\Pi_{1,i,j}(x) = \frac{\Gamma_{1,i,j}(x)}{\Omega_{2,i,j}(x)}, \text{ where} \tag{23}$$

$$
\begin{aligned}
\Gamma_{1,i,j}(x) &= T^*_{i,j,1}\theta^4 + T^*_{i,j,2}\theta^3(1-\theta) + T^*_{i,j,3}\theta^2(1-\theta)^2 \\
&\quad + T^*_{i,j,4}\theta(1-\theta)^3 + T^*_{i,j,5}(1-\theta)^4, \\
T^*_{i,j,1} &= z^x_{i+1,j} - k_{x,1,j} - \frac{\alpha_{i,j}}{h_i}(x_m - x_1)(z^x_{m,j} - k_{x,1,j}), \\
T^*_{i,j,2} &= 2\Big[\tau^*_{i,j}(\triangle_{i,j} - k_{x,1,j}) - (z^x_{i,j} - k_{x,1,j})\Big] \\
&\quad - \frac{2\alpha_{i,j}}{h_i}\Big[\tau^*_{i,j}(z_{m,j} - z_{1,j} - k_{x,1,j}) - (z^x_{1,j} - k_{x,1,j})(x_m - x_1)\Big], \\
T^*_{i,j,3} &= (\tau^{*2}_{i,j} + 3)(\triangle_{i,j} - k_{x,1,j}) - \tau^*_{i,j}\big[z^x_{i,j} - k_{x,1,j} + z^x_{i+1,j} - k_{x,1,j}\big] \\
&\quad - \frac{\alpha_{i,j}}{h_i}\Big[(\tau^{*2}_{i,j} + 3)\big(z_{m,j} - z_{1,j} - k_{x,1,j}\big) \\
&\quad - \tau^*_{i,j}(x_m - x_1)\big[z^x_{1,j} - k_{x,1,j} + z^x_{m,j} - k_{x,1,j}\big]\Big], \\
T^*_{i,j,4} &= 2\big[\tau^*_{i,j}(\triangle_{i,j} - k_{x,1,j}) - (z^x_{i+1,j} - k_{x,1,j})\big] \\
&\quad - \frac{2\alpha_{i,j}}{h_i}\big[\tau^*_{i,j}(z_{m,j} - z_{1,j} - k_{x,1,j}) - (z^x_{m,j} - k_{x,1,j})(x_m - x_1)\big], \\
T^*_{i,j,5} &= z^x_{i,j} - k_{x,1,j} - \frac{\alpha_{i,j}}{h_i}(x_m - x_1)(z^x_{1,j} - k_{x,1,j}), \\
\tau^*_{i,j} &= 1 + \frac{h_i\big[z^x_{i,j} - k_{x,1,j} + z^x_{i+1,j} - k_{x,1,j}\big]}{h_i(\triangle_{i,j} - k_{x,1,j}) - \alpha_{i,j}\big[z_{m,j} - z_{1,j} - k_{x,1,j}\big]} \\
&\quad - \frac{\alpha_{i,j}(x_m - x_1)\big[z^x_{1,j} - k_{x,1,j} + z^x_{m,j} - k_{x,1,j}\big]}{h_i(\triangle_{i,j} - k_{x,1,j}) - \alpha_{i,j}\big[z_{m,j} - z_{1,j} - k_{x,1,j}\big]}.
\end{aligned}
$$

Since $\Omega_{2,i,j}(x) > 0$ for all $x \in I$, $\Pi_{1,i,j}(x) \geq 0$ if and only if $\Gamma_{1,i,j}(x) \geq 0$ for all $x \in I$. From (23), $\Gamma_{1,i,j}(x) \geq 0$ if $T^*_{i,j,l} \geq 0, l = 1, 2, \ldots, 5$. Again from (23), we observe that $T^*_{i,j,1} \geq 0$ and $T^*_{i,j,5} \geq 0$ if

$$
\alpha_{i,j} \leq \min\Big\{\frac{a_i(z^x_{i+1,j} - k_{x,1,j})}{z^x_{m,j} - k_{x,1,j}}, \frac{a_i(z^x_{i,j} - k_{x,1,j})}{z^x_{1,j} - k_{x,1,j}}\Big\}. \tag{24}
$$

Expressing $\tau^*_{i,j}$ in terms of $T^*_{i,j,1}$ and $T^*_{i,j,5}$, we have

$$
\tau^*_{i,j} = 1 + \frac{h_i(T^*_{i,j,1} + T^*_{i,j,5})}{h_i(\triangle_{i,j} - k_{x,1,j}) - \alpha_{i,j}\big[z_{m,j} - z_{1,j} - k_{x,1,j}\big]}. \tag{25}
$$

We can observe that (24) implies $T^*_{i,j,1} + T^*_{i,j,5} \geq 0$. Therefore, including (24), $\tau^*_{i,j} \geq 0$ whenever

$$
\alpha_{i,j} < \frac{h_i(\triangle_{i,j} - k_{x,1,j})}{z_{m,j} - z_{1,j} - k_{x,1,j}}. \tag{26}
$$

Now from (24)-(26), it is easy to notice that

$$
\begin{aligned}
&\tau^*_{i,j} \geq \frac{h_i T^*_{i,j,5}}{h_i(\triangle_{i,j} - k_{x,1,j}) - \alpha_{i,j}(z_{m,j} - z_{1,j} - k_{x,1,j})} \\
&\Rightarrow \tau^*_{i,j}[\triangle_{i,j} - k_{x,1,j} - \frac{\alpha_{i,j}}{h_i}(z_{m,j} - z_{1,j} - k_{x,1,j})] \geq T^*_{i,j,5} \\
&\Rightarrow T^*_{i,j,2} \geq 0.
\end{aligned}
$$

Similarly using (24)-(26), we conclude that $T^*_{i,j,4} \geq 0$. Again from (24)-(26), we have the following inequality:

$$
\tau^*_{i,j} \geq \frac{h_i(T^*_{i,j,1} + T^*_{i,j,5})}{h_i(\triangle_{i,j} - k_{x,1,j}) - \alpha_{i,j}\big[z_{m,j} - z_{1,j} - k_{x,1,j}\big]}.
$$

$$\Rightarrow \tau_{i,j}^{*2}\Big(\triangle_{i,j} - k_{x,1,j} - \frac{\alpha_{i,j}}{h_i}\big[z_{m,j} - z_{1,j} - k_{x,1,j}\big]\Big) \geq \tau_{i,j}^{*}(T_{i,j,1}^{*} + T_{i,j,5}^{*}). \tag{27}$$

The inequality (26) is re-written as

$$3\frac{\alpha_{i,j}}{h_i}(z_{m,j} - z_{1,j} - k_{x,1,j}) < 3(\triangle_{i,j} - k_{x,1,j}), \tag{28}$$

and from (23), we have

$$\begin{aligned} T_{i,j,3}^{*} =& \tau_{i,j}^{*2}\big[\triangle_{i,j} - k_{x,1,j} - \frac{\alpha_{i,j}}{h_i}(z_{m,j} - z_{1,j} - k_{x,1,j})\big] - \tau_{i,j}^{*}(T_{i,j,1}^{*} + T_{i,j,5}^{*}) \\ &+ 3\Big(\triangle_{i,j} - k_{x,1,j} - \frac{\alpha_{i,j}}{h_i}\big[z_{m,j} - z_{1,j} - k_{x,1,j}\big]\Big). \end{aligned} \tag{29}$$

Now using (27)-(28), it is easy to verify from (29) that $T_{i,j,3}^{*} \geq 0$.
Thus, $\Pi_{1,i,j}(x) \geq 0 \; \forall \; x \in I, \; i = 1, 2, \ldots, m-1, j = 1, 2, \ldots, n$, if

$$\alpha_{i,j} \in \Big[0, \; \min\{\frac{a_i(z_{i+1,j}^{x} - k_{x,1,j})}{z_{m,j}^{x} - k_{x,1,j}}, \frac{a_i(z_{i,j}^{x} - k_{x,1,j})}{z_{1,j}^{x} - k_{x,1,j}}, \frac{h_i(\triangle_{i,j} - k_{x,1,j})}{z_{m,j} - z_{1,j} - k_{x,1,j}}, a_i\}\Big).$$

Proceeding in the similar way as above, we have found that $\Pi_{2,i,j}(x) \leq 0 \forall x \in I, \; i = 1, 2, \ldots, m-1, j = 1, 2, \ldots, n$, if

$$\alpha_{i,j} \in \Big[0, \; \min\{\frac{a_i(k_{x,2,j} - z_{i+1,j}^{x})}{k_{x,2,j} - z_{m,j}^{x}}, \frac{a_i(k_{x,2,j} - z_{i,j}^{x})}{k_{x,2,j} - z_{1,j}^{x}}\}, \frac{h_i(k_{x,2,j} - \triangle_{i,j})}{k_{x,2,j} - (z_{m,j} - z_{1,j})}, a_i\}\Big).$$

Combining the above restrictions on $\alpha_{i,j}$, the fractal boundary curve $B_j(x)$ is monotonically increasing over I for $j = 1, 2, \ldots, n$ if

$$\alpha_{i,j} \in [0, \lambda_{x,i,j}), i = 1, 2, \ldots, m-1.$$

Case-II For differentiability of B_j, we have $-a_i < \alpha_{i,j} \leq 0, i = 1, 2, \ldots, m-1, j = 1, 2, \ldots, n$. As per our assumptions, $k_{x,1,j} \leq z^d \leq k_{x,2,j}, j = 1, 2, \ldots, n$. Combining these inequalities, we obtain $\frac{k_{x,2,j}\alpha_{i,j}}{a_i} \leq \frac{z^d\alpha_{i,j}}{a_i} \leq \frac{k_{x,1,j}\alpha_{i,j}}{a_i}, j = 1, 2, \ldots, n$. Hence, we can write

$$\frac{k_{x,2,j}\alpha_{i,j}}{a_i} + \frac{\Omega_{1,i,j}(x)}{a_i\Omega_{2,i,j}(x)} \leq \frac{z^d\alpha_{i,j}}{a_i} + \frac{\Omega_{1,i,j}(x)}{a_i\Omega_{2,i,j}(x)} \leq \frac{\alpha_{i,j}k_{x,1,j}}{a_i} + \frac{\Omega_{1,i,j}(x)}{a_i\Omega_{2,i,j}(x)}, \tag{30}$$

for $i = 1, 2, \ldots, m-1, j = 1, 2, \ldots, n$. From (30), it is easy to see that $F_{i,j}^{d}(x, z^d) \in [k_{x,1,j}, k_{x,2,j}] \;\; \forall (x, z^d) \in I \times [k_{x,1,j}, k_{x,2,j}], \; i = 1, 2, \ldots, m-1, j = 1, 2, \ldots, n$, if

- $\Pi_{1,i,j}^{*}(x) := \frac{k_{x,2,j}\alpha_{i,j} - a_ik_{x,1,j}}{a_i} + \frac{\Omega_{1,i,j}(x)}{a_i\Omega_{2,i,j}(x)} \geq 0,$
- $\Pi_{2,i,j}^{*}(x) := \frac{k_{x,1,j}\alpha_{i,j} - a_ik_{x,2,j}}{a_i} + \frac{\Omega_{1,i,j}(x)}{a_i\Omega_{2,i,j}(x)} \leq 0.$

Applying similar argument as in $\Pi_{1,i,j}(x) \geq 0 \; \forall x \in I$, we have found that $\Pi_{1,i,j}^{*}(x) \geq 0 \; \forall x \in I, \; i = 1, 2, \ldots, m-1, j = 1, 2, \ldots, n$, if

$$\alpha_{i,j} \in \Big(\max\{\frac{-a_i(z_{i+1,j}^{x} - k_{x,1,j})}{k_{x,2,j} - z_{m,j}^{x}}, \frac{-a_i(z_{i,j}^{x} - k_{x,1,j})}{k_{x,2,j} - z_{1,j}^{x}}, \frac{-h_i(\triangle_{i,j} - k_{x,1,j})}{k_{x,2,j} - (z_{m,j} - z_{1,j})}, -a_i\}, 0\Big].$$

Similarly, we have found that $\Pi_{2,i,j}^{*}(x) \leq 0 \; \forall x \in I, \; i = 1, 2, \ldots, m-1, j = 1, 2, \ldots, n, \;$ if

$$\alpha_{i,j} \in \Big(\max\{\frac{-a_i(k_{x,2,j} - z_{i+1,j}^{x})}{z_{m,j}^{x} - k_{x,1,j}}, \frac{-a_i(k_{x,2,j} - z_{i,j}^{x})}{z_{1,j}^{x} - k_{x,1,j}}, \frac{-h_i(k_{x,2,j} - \triangle_{i,j})}{z_{m,j} - z_{1,j} - k_{x,1,j}}, -a_i\}, \; 0\Big].$$

Combining the restrictions on $\alpha_{i,j}$ in this case, the fractal boundary curve B_j is monotonically increasing over I for $j = 1, 2, \ldots, n$, if

$$\alpha_{i,j} \in (\lambda_{x,i,j}^{*}, 0], i = 1, 2, \ldots, m-1.$$

From Case-I and Case-II, the fractal boundary curve B_j is monotonically increasing over I if the scaling parameters are chosen according to (19). Similarly, the above result is extended to the fractal boundary curve B_i^*. Hence B_i^* is monotonically increasing over J if the scaling parameters $\alpha_{i,j}^*$, $j = 1, 2, \ldots, n-1$, are selected with respect to (20). Since all the fractal boundary curves (11) and (13) are monotonically increasing for the scaling parameters chosen according to (19) and (20) respectively, as per the observation by Casciola and Romani [8], the rational quadratic fractal interpolation surface Ψ (16) is monotonically increasing over the domain D. For a monotonically decreasing surface data set, the above procedure yields the same optimal range restrictions on the scaling parameters to obtain the monotonically decreasing rational quadratic FISs. It completes the proof. □

Remark 4.1. *For given monotonic surface data, if* $\triangle_{i,j} \neq 0, i = 1, 2, \ldots, m-1, j = 1, 2, \ldots, n$, $\triangle_{i,j}^* \neq 0, i = 1, 2, \ldots, m, j = 1, 2, \ldots, n-1$, *and the scaling matrices* α *and* α^* *are chosen with respect to (19) and (20) respectively, then it is easy to observe that* $sgn(q_{i,j}(\theta)) = sgn(\triangle_{i,j})$ *and* $sgn(q_{i,j}^*(\phi)) = sgn(\triangle_{i,j}^*)$. *Thus,* $q_{i,j}(\theta) \neq 0$ *for* $\theta \in [0, 1]$ *and* $q_{i,j}^*(\phi) \neq 0$ *for* $\phi \in [0, 1]$. *So, our construction of quadratic FIS is valid for any monotonic rectangular surface data.*

4.2. Symmetric Rational Quadratic FIS. The following theorem addresses the condition on the scaling parameters for the symmetricity preserving rational quadratic FISs for the given symmetric data.

Theorem 4.2. *Let* $\{(x_i, y_j, z_{i,j}, z_{i,j}^x, z_{i,j}^y) : i, j = 1, 2, \ldots, m\}$ *be a symmetric data set, i.e.,* $x_l = y_l, l = 1, 2, \ldots, m$, $z_{i,j} = z_{j,i}$, $z_{i,j}^x = z_{j,i}^y$, $i, j = 1, 2, \ldots, m$, *if the matrices of the scaling parameters* α *and* α^* *satisfy the relation* $\alpha = \alpha^{*T}$, *then the* $\mathcal{C}^1$*-rational quadratic FIS* Ψ *is symmetric about the plane* $y = x$.

Proof. For the above symmetric surface data, the x-direction and y-direction homeomorphisms are same in the IFSs (12) and (14). This implies that

$$a_{x,0}(\theta) = b_{y,0}(\phi), a_{x,1}(\theta) = b_{y,1}(\phi). \tag{31}$$

Again for given symmetric surface data, we have $T_l = T_l^*, l = 1, 2, \ldots, m$. Using this observation in IFSs (12) and (14), for $l = 1, 2, \ldots, m$, we observe that

$$B_l(x) = B_l^*(y) \text{ whenever } \alpha = \alpha^{*T}. \tag{32}$$

Now using (31) and (32), we have

$$\begin{aligned}
\Psi(x, y) =& b_{y,0}(\phi)B_j(x) + b_{y,1}(\phi)B_{j+1}(x) + a_{x,0}(\theta)B_i^*(y) + a_{x,1}(\theta)B_{i+1}^*(y) \\
&- a_{x,0}(\theta)b_{y,0}(\phi)z_{i,j} - a_{x,0}(\theta)b_{y,1}(\phi)z_{i,j+1} - a_{x,1}(\theta)b_{y,0}(\phi)z_{i+1,j} \\
&- a_{x,1}(\theta)b_{y,1}(\phi)z_{i+1,j+1}, \\
=& a_{x,0}(\theta)B_i^*(y) + a_{x,1}(\theta)B_{i+1}^*(y) + b_{y,0}(\phi)B_j(x) + b_{y,1}(\phi)B_{j+1}(x) \\
&- b_{y,0}(\phi)a_{x,0}(\theta)z_{j,i} - b_{y,0}(\phi)a_{x,1}(\theta)z_{j,i+1} - b_{y,1}(\phi)a_{x,0}(\theta)z_{j+1,i} \\
&- b_{y,1}(\phi)a_{x,1}(\theta)z_{j+1,i+1}, \\
=& \Psi(y, x).
\end{aligned}$$

Thus, the rational quadratic FIS Ψ is symmetric in the given domain D whenever $\alpha = \alpha^{*T}$. It completes the proof. □

Remark 4.2. *For a monotonic surface data, the monotonic symmetric rational quadratic FISs can be obtained with a choice of* $\alpha = \alpha^{*T}$ *according to Theorem 4.1. When we relax the above condition* $\alpha = \alpha^{*T}$, *we obtain a monotonic non-symmetric rational quadratic FIS. Hence our fractal technique provides both symmetric and*

non-symmetric rational quadratic FISs due to the presence of scaling factors in its structure. But the corresponding classical interpolant provides only a symmetric surface as $\alpha = \alpha^{*T} = [0]_{(m-1)\times m}$.

5. Examples and Discussion

In order to illustrate the comprehensive visual quality of the $\mathcal{C}^1$-rational quadratic spline FISs in fitting a monotonic/symmetric surfaces, consider the increasing and symmetric surface data given in Table 1 (cf. Section 1). For this surface data, according to Theorem 4.1, we choose $k_{x,1,j} = 0, k_{x,2,j} = 650, j = 1, 2, 3, 4$, and $k_{y,1,i} = 0, k_{y,2,i} = 650, i = 1, 2, 3, 4$. To generate monotonically increasing quadratic FIS Ψ (cf. (16)), we determine the matrices of the scaling parameters according to (19) and (20). Details of the scaling matrices used in the construction of all the fractal boundary curves in Figs. 2(a)-(f) are given in Table 2.

TABLE 2. Matrices of the scaling parameters used in the construction of the fractal boundary curves.

Figs.	Matrices of scaling parameters (α/α^*)	Figs.	Matrices of scaling parameters (α/α^*)
2(a)	$\alpha = \alpha^{*T} = \begin{bmatrix} 0.15 & 0.23 & 0.3 \\ 0.15 & 0.23 & 0.3 \\ 0.15 & 0.23 & 0.3 \\ 0.15 & 0.23 & 0.3 \end{bmatrix}^T$	2(d)	$\alpha = \alpha^{*T} = \begin{bmatrix} -0.02 & -0.1 & -0.02 \\ -0.1 & -0.1 & -0.02 \\ -0.1 & -0.03 & -0.003 \\ -0.01 & -0.02 & -0.004 \end{bmatrix}^T$
2(b)	$\alpha = \alpha^{*T} = \begin{bmatrix} 0.01 & 0.01 & 0.01 \\ 0.01 & 0.01 & 0.01 \\ 0.15 & 0.23 & 0.3 \\ 0.15 & 0.23 & 0.3 \end{bmatrix}^T$	2(e)	$\alpha = \begin{bmatrix} 0.15 & 0.23 & 0.3 \\ 0.15 & 0.23 & 0.3 \\ 0.15 & -0.0035 & 0.3 \\ 0.15 & -0.0043 & -0.0042 \end{bmatrix}^T$
2(c)	$\alpha = \alpha^{*T} = \begin{bmatrix} 0.15 & 0.23 & 0.3 \\ 0.15 & 0.23 & 0.3 \\ 0.01 & 0.01 & 0.01 \\ 0.01 & 0.01 & 0.01 \end{bmatrix}^T$	2(f)	$\alpha^* = \begin{bmatrix} 0.15 & 0.23 & 0.3 \\ 0.15 & -0.002 & -0.002 \\ 0.15 & 0.23 & 0.3 \\ 0.15 & 0.23 & 0.3 \end{bmatrix}$

For the given surface data, the homeomorphisms in x-direction are $L_1(x) = \frac{1}{3}x + \frac{2}{3}, L_2(x) = \frac{1}{3}x + \frac{5}{3}$, and $L_3(x) = \frac{1}{3}x + \frac{8}{3}$. The matrices α of the scaling parameters given in Table 2 are used in IFSs $\mathcal{I}_j, j = 1, 2, 3, 4$ (cf. (12)) to generate increasing fractal boundary curves iteratively in x-direction that interpolates the data sets $T_1 = \{(1, 1, 1), (2, 2, 2), (3, 3, 3), (4, 4, 4)\}, T_2$=$\{(1, 2, 4), (2, 4, 8), (3, 6, 12), (4, 8, 16)\}, T_3 = \{(1, 3, 9), (2, 6, 18), (3, 9, 27), (4, 12, 36)\}$, and $T_4 = \{(1, 4, 16), (2, 8, 32), (3, 12, 48), (4, 16, 64)\}$. For the given symmetric surface data, the homeomorphisms $L_i^*(y)$ in y-direction are same as $L_j(x)$ for $i = j$, $i = 1, 2, 3$. The scaling matrices α^* given in Table 2 are used in IFSs $\mathcal{I}_i^*, i = 1, 2, 3, 4$ (cf. (14)) to generate the y-direction increasing fractal boundary curves iteratively that interpolates the data sets $T_1^* = T_1, T_2^* = T_2$, $T_3^* = T_3$, and $T_4^* = T_4$. According to Theorem 4.2, the fractal boundary curves in x-direction and y-direction match whenever $\alpha = \alpha^{*T}$. Owing to this reason, we have generated both x-direction and y-direction fractal boundary curves in Figs. 2(a)-(c) with the choice $\alpha = \alpha^{*T}$. By comparing Fig. 2(a) and Fig. 2(b), we can observe the effects of scaling parameters in the fractal boundary curves $B_1(x) = B_1^*(y)$ and $B_2(x) = B_2^*(y)$. Next a comparison between Fig. 2(a) and Fig. 2(c) reveals the role of scaling parameters in modifying the shape of the fractal boundary curves $B_3(x) = B_3^*(y)$ and $B_4(x) = B_4^*(y)$. The fractal boundary curves in Fig. 2(d) are obtained by modifying the scaling factors in negative direction for all fractal boundary curves in Fig. 2(a). Next, the x-direction fractal boundary curves in Fig. 2(e) are generated using the scaling matrix α (see Table 2) in the IFS (12). Similarly, the y-direction fractal boundary curves in Fig. 2(f) are constructed using the scaling matrix α^*

(see Table 2) in the IFS (14). The x-direction fractal boundary curves in Fig. 2(e) and y-direction fractal boundary curves in Fig. 2(f) are not identical because the scaling matrices used in their construction violating the relation $\alpha = \alpha^{*T}$ (see Table 2).

Utilizing the above constructed fractal boundary curves through (16), we construct the rational quadratic FISs in Figs. 3(a)-(g). Using the fractal boundary curves in Fig. 2(a) in (16), a $\mathcal{C}^1$-rational quadratic FIS is computed and plotted in Fig. 3(a). Next we generate an increasing rational quadratic FIS in Fig. 3(b) by availing the fractal boundary curves in Fig. 2(b) through (16). By comparing the FIS in Fig. 3(b) with the FIS in Fig. 3(a), visually pleasing changes are observed in the surface patch pertaining to $[1,4]\times[1,2]$ and $[1,2]\times[1,4]$, and changes in rest of the surface are negligible. Similarly, we construct a $\mathcal{C}^1$-rational quadratic FIS in Fig. 3(c) with the choice of fractal boundary curves in Fig. 2(c). Furthermore, eye-catching changes are observed almost every where in the FIS in Fig. 3(c) when compared with the FIS in Fig. 3(a). The quadratic FISs in Figs. 3(a)-(c) are monotonically increasing and symmetric in nature.

Now we generate an increasing non-symmetric rational quadratic FIS in Fig. 3(d) with fractal boundary curves as in Figs. 2(e)-2(f) in (16). When the FIS in Fig. 3(d) compared with the FIS in Fig. 3(a), we have found visually pleasing changes in the fractal surface pertaining to $[1,4]\times[3,4]$. A rational quadratic FIS is generated iteratively in Fig. 3(e) by using the fractal boundary curves: Fig. 2(d) in x-direction and Fig. 2(f) in y-direction. The qualitative changes in the shape of Fig. 3(e) are observed by comparing it with Fig. 3(a) and Fig. 3(d). Another rational quadratic FIS is generated in Fig. 3(f) by using the fractal boundary curves: Fig. 2(e) in x-direction and Fig. 2(d) in y-direction. It is easy to notice that the rational quadratic FISs in Fig. 3(f) and Fig. 3(c) look alike except for the surface patch pertaining to $[1,2]\times[3,4]$. The last increasing rational quadratic FIS is obtained in Fig. 3(g) using the fractal boundary curves in Fig. 2(a) and Fig. 2(c) in x-direction and y-direction respectively in (16). The rational quadratic FIS in Fig. 3(g) is similar to the mirror image of the rational quadratic FIS in Fig. 3(e). Finally, a rational quadratic FIS in Fig. 3(h) is generated with the arbitrary selection of the scaling parameters as $\alpha = [0.1]_{3\times 4}$ and $\alpha^* = [-0.25]_{4\times 3}$ in (16). It is easy to visualize that rational quadratic FIS in Fig. 3(h) is not increasing as α and α^* do not satisfy the conditions of Theorem 4.1. This observation demonstrates the importance of Theorems 4.1-4.2 in acquiring monotonic (symmetric/non-symmetric) rational quadratic FISs for a given monotonic and symmetric surface data.

The rational quadratic FISs in Figs.3(d)-(g) are not symmetric with respect to the plane $y = x$ as $\alpha \neq \alpha^{*T}$. From the above examples, we can conclude that whenever there is a change in the x-direction or y-direction fractal boundary curves, we will have the changes in the corresponding $\mathcal{C}^1$-rational quadratic FIS. By varying the matrices of scaling parameters, it is possible to simulate monotonic surfaces that are symmetric/non-symmetric in nature. For a given surface, an optimal rational quadratic FIS can be obtained by using optimization methods like genetic algorithm or evolution program for appropriate scaling matrices.

6. Convergence Analysis of Monotonic Rational Quadratic FIS

In this section, an upper bound of the error between the monotonic rational quadratic FIS Ψ and an original function $\Phi \in \mathcal{C}^4(D)$ is estimated. We use the notation: $|\alpha_j|_\infty := \max\{|\alpha_{i,j}| : i = 1,2,\ldots,m-1\}, j = 1,2,\ldots,n$, $|\alpha|_\infty := \max\{|\alpha_j|_\infty : j = 1,2,\ldots,n\}$, $h = \max\{h_i : i = 1,2,\ldots,m-1\}$; $|\alpha_i^*|_\infty := \max\{|\alpha_{i,j}^*| :$

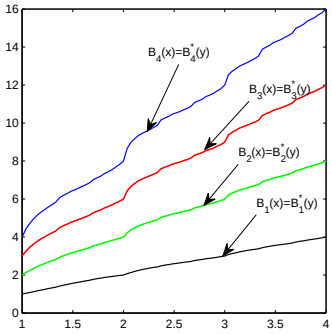

(a): Increasing fractal boundary curves in x-direction and y-direction.

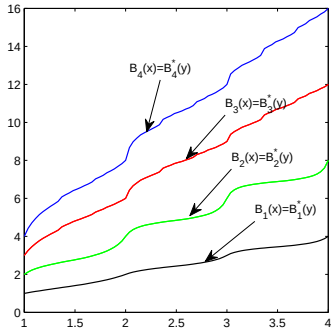

(b): Effects of change in $\alpha = \alpha^{*T}$ in $B_1(x) = B_1^*(y)$ and $B_2(x) = B_2^*(y)$ of Fig. 2(a).

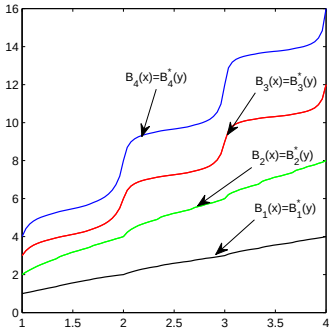

(c): Effects of change in $\alpha = \alpha^{*T}$ in $B_3(x) = B_3^*(y)$ and $B_4(x) = B_4^*(y)$ of Fig. 2(a).

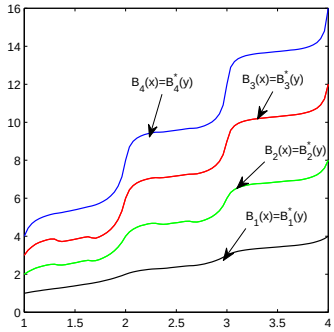

(d): Fractal boundary curves in x-direction and y-direction with negative scaling parameters.

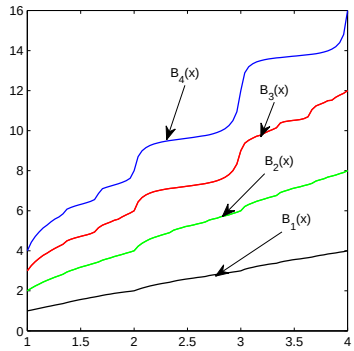

(e): Fractal boundary curves in x-direction.

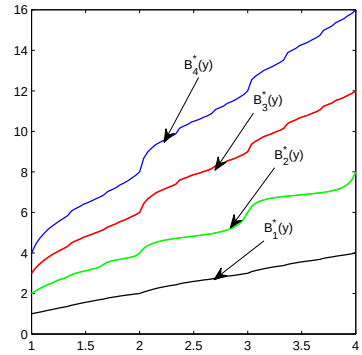

(f): Fractal boundary curves in y-direction.

FIGURE 2. Rational quadratic fractal boundary curves.

$j = 1, 2, \ldots, n-1\}, i = 1, 2, \ldots, m$, $|\alpha^*|_\infty := \max\{|\alpha_i^*|_\infty : i = 1, 2, \ldots, m\}$, $h^* = \max\{h_j^* : j = 1, 2, \ldots, n-1\}$ in the following theorem:

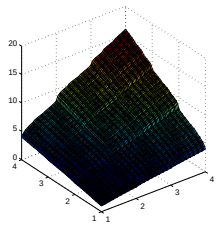

(a): Increasing symmetric rational quadratic spline FIS using Fig. 3(a).

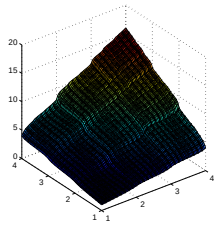

(b): Increasing symmetric rational quadratic FIS using Fig. 3(b).

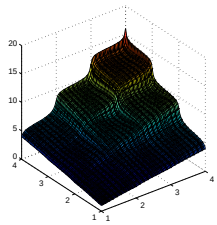

(c): Increasing symmetric rational quadratic FIS using Fig. 3(c).

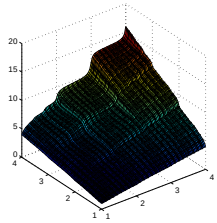

(d): Increasing non-symmetric rational quadratic FIS using Figs. 3(e)-(f).

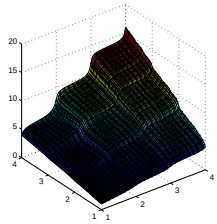

(e): Increasing non-symmetric rational quadratic FIS using Figs. 3(d) and 3(f).

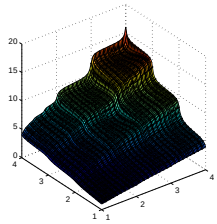

(f): Increasing non-symmetric rational quadratic FIS using Figs. 3(e) and 3(d).

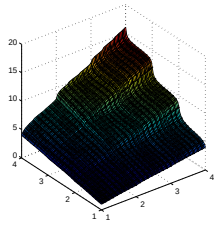

(g): Increasing non-symmetric rational quadratic FIS using Figs. 3(a) and 3(c).

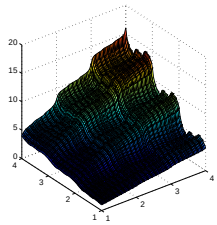

(h): Non-increasing rational quadratic FIS.

FIGURE 3. $\mathcal{C}^1$-rational quadratic FISs.

Theorem 6.1. *Let Ψ and S, respectively be the monotonic rational quadratic FIS and classical monotonic rational quadratic spline surface interpolant for the monotonic surface data $\{(x_i, y_j, z_{i,j}) : i = 1, 2, \ldots, m,\ j = 1, 2, \ldots, n\}$ generated from an*

original function $\Phi \in \mathcal{C}^4(D)$. Let the partial derivatives $z^x_{i,j}, z^y_{i,j}, i = 1, 2, \ldots, m, j = 1, 2, \ldots, n$, satisfy the necessary conditions for monotonicity, and the scaling matrices α and α^* are selected with respect to (19) and (20) respectively. Then

$$\begin{aligned}\big\|\Phi - \Psi\big\|_\infty \leq & \frac{2|\alpha|_\infty}{1-|\alpha|_\infty}\ (\Lambda_x + U_x(\alpha)) + \frac{2|\alpha^*|_\infty}{1-|\alpha^*|_\infty}\ (\Lambda_y + U_y(\alpha^*)) + h\Big\|\frac{\partial \Phi}{\partial x}\Big\|_\infty \\ & + h\Big\|\frac{\partial S}{\partial x}\Big\|_\infty + h^* \max_{1\leq i\leq m} A_i(\Phi) \max_{1\leq i\leq m}\Big[\max_{1\leq j\leq n-1}\Big\{\Big|\frac{\partial \Phi(x_i, y_j)}{\partial y} - z^y_{i,j}\Big|, \\ & \Big|\frac{\partial \Phi(x_i, y_{j+1})}{\partial y} - z^y_{i,j+1}\Big|\Big\}\Big] + h^{*4} \max_{1\leq i\leq m}\Big\{\max_{1\leq j\leq n-1} B_{i,j}(\Phi)\Big\},\end{aligned}$$

where $B_{i,j}(\Phi) = \frac{1}{384c_i^*}\{\|\frac{\partial \Phi_i}{\partial y}\|_\infty \|\frac{\partial^4 \Phi_i}{\partial y^4}\|_\infty + \frac{2}{3}h_j^* \|\frac{\partial^4 \Phi_i}{\partial y^4}\|^2_\infty + 2\|\frac{\partial^2 \Phi_i}{\partial y^2}\|_\infty \|\frac{\partial^3 \Phi_i}{\partial y^3}\|_\infty\}$,

$$\Big\|\frac{\partial^k \Phi_i}{\partial y^k}\Big\|_\infty = \max\Big\{\Big|\frac{\partial^k \Phi(x_i, y)}{\partial y^k}\Big|; y \in J\Big\}, k = 1, 2, 3, 4, A_i(\Phi) = \frac{\|\frac{\partial \Phi_i}{\partial y}\|_\infty}{4c_i^*},$$

c_i^* is constant such that $\min_{0\leq\phi\leq 1} |E_{i,j}(\phi)| \geq c_i^* > 0$,
$E_{i,j}(\phi) = \triangle^*_{i,j}\phi^2 + (z^y_{i,j} + z^y_{i,j+1})\phi(1-\phi) + \triangle^*_{i,j}(1-\phi)^2$,
and the constants Λ_x, $U_x(\alpha)$, Λ_y, $U_y(\alpha^*)$ are defined in the proof.

Proof. Since Ψ and S, respectively are the monotonic rational quadratic FIS and the classical monotonic rational quadratic spline surface interpolant with respect to the given monotonic surface data, from (16) and Remark 3.1, we have

$$\left\{\begin{array}{l} |\Psi(x,y) - S(x,y)| \leq b_{y,0}(\phi)\|B_j - S_j\|_\infty + b_{y,1}(\phi)\|B_{j+1} - S_{j+1}\|_\infty \\ \qquad\qquad + a_{x,0}(\theta)\|B_i^* - S_i^*\|_\infty + a_{x,1}(\theta)\|B_{i+1}^* - S_{i+1}^*\|_\infty. \end{array}\right. \tag{33}$$

Using the error estimation between the rational quadratic FIF and the classical quadratic interpolant S_j, from [cf. Theorem 10, [13]], we have

$$\|B_j - S_j\|_\infty \leq \frac{|\alpha_j|_\infty}{1-|\alpha_j|_\infty}(\Lambda_{x,j} + U_{x,j}(\alpha)), j = 1, 2, \ldots, n, \tag{34}$$

$$\begin{aligned}\Lambda_{x,j} &= \max_{1\leq i\leq m-1}\{2(|z_{i,j}| + |z_{i+1,j}|)\}, \\ U_{x,j}(\alpha) &= \max_{1\leq i\leq m-1}\{U^*_{x,i,j}(\alpha) + V^*_{x,i,j}(\alpha)W^*_{x,i,j}(\alpha)\}, \\ U^*_{x,i,j}(\alpha) &= 2|z_{m,j} - z_{1,j}| + |z_{1,j}| + |z_{m,j}| + \frac{|u_{x,4,i,j} + 2\alpha_{i,j}u_{x,5,i,j}|}{|\pi_{x,2,i,j} - \pi_{x,1,i,j}|}, \\ V^*_{x,i,j}(\alpha) &= |u_{x,2,i,j}| + |u_{x,1,i,j}| + \frac{|u_{x,3,i,j}a_i + \alpha_{i,j}u_{x,4,i,j} + \alpha^2_{i,j}u_{x,5,i,j}|}{|\pi_{x,2,i,j} - \pi_{x,1,i,j}|}, \\ W^*_{x,i,j}(\alpha) &= \frac{2|z_{m,j} - z_{1,j}|}{|u_{x,2,i,j} - u_{x,1,i,j}|} + \frac{|z^x_{1,j} + z^x_{m,j}|}{|\pi_{x,2,i,j} - \pi_{x,1,i,j}|}, \\ \pi_{x,1,i,j} &= a_i z^x_{i,j} - \alpha_{i,j}z^x_{1,j}, \pi_{x,2,i,j} = a_i z^x_{i+1,j} - \alpha_{i,j}z^x_{m,j}, \\ u_{x,1,i,j} &= z_{i,j} - \alpha_{i,j}z_{1,j}, u_{x,2,i,j} = z_{i+1,j} - \alpha_{i,j}z_{m,j}, \\ u_{x,3,i,j} &= z_{i,j}z^x_{i+1,j} + z_{i+1,j}z^x_{i,j}, u_{x,5,i,j} = z_{m,j}z^x_{1,j} + z_{1,j}z^x_{m,j}, \\ u_{x,4,i,j} &= -[z_{i+1,j}z^x_{1,j} + z_{i,j}z^x_{m,j} + a_i(z_{m,j}z^x_{i,j} + z_{1,j}z^x_{i+1,j})].\end{aligned}$$

By re-iterating the above procedure for B_i^*, from [13], we obtain

$$\|B_i^* - S_i^*\|_\infty \leq \frac{|\alpha_i^*|_\infty}{1-|\alpha_i^*|_\infty}(\Lambda_{y,i} + U_{y,i}(\alpha^*)), i = 1, 2, \ldots, m, \tag{35}$$

$\Lambda_{y,i}$ and $U_{y,i}(\alpha^*)$ are similar to the $\Lambda_{x,j}$ and $U_{x,j}(\alpha)$ respectively. Since the blending functions $a_{x,0}, a_{x,1}, b_{y,0}, b_{y,1}$ are bounded by 1, using (34) and (35) in (33), we have

$$\begin{aligned}|\Psi(x,y)-S(x,y)| &\leq \frac{|\alpha_j|_\infty}{1-|\alpha_j|_\infty}(\Lambda_{x,j}+U_{x,j}(\alpha))+\frac{|\alpha_{j+1}|_\infty}{1-|\alpha_{j+1}|_\infty}(\Lambda_{x,j+1}+U_{x,j+1}(\alpha))\\ &\quad+\frac{|\alpha_i^*|_\infty}{1-|\alpha_i^*|_\infty}(\Lambda_{y,i}+U_{y,i}(\alpha^*))+\frac{|\alpha_{j+1}^*|_\infty}{1-|\alpha_{j+1}^*|_\infty}(\Lambda_{y,i+1}+U_{y,i+1}(\alpha^*))\\ &\leq \frac{2|\alpha|_\infty}{1-|\alpha|_\infty}(\Lambda_x+U_x(\alpha))+\frac{2|\alpha^*|_\infty}{1-|\alpha^*|_\infty}(\Lambda_y+U_y(\alpha^*)),\end{aligned}$$

where $\Lambda_x=\max\limits_{1\leq j\leq n}\Lambda_{x,j}$, $U_x(\alpha)=\max\limits_{1\leq j\leq n}U_{x,j}(\alpha)$, Λ_y and $U_y(\alpha^*)$ are defined similar to Λ_x and $U_x(\alpha)$ respectively. Since the above inequality is true for every $(x,y)\in D_{i,j}, i=1,2,\ldots,m-1, j=1,2,\ldots,n-1$, we get the following estimation:

$$\|\Psi-S\|_\infty \leq \frac{2|\alpha|_\infty}{1-|\alpha|_\infty}(\Lambda_x+U_x(\alpha))+\frac{2|\alpha^*|_\infty}{1-|\alpha^*|_\infty}(\Lambda_y+U_y(\alpha^*)). \tag{36}$$

Expanding the classical rational quadratic FIS $S\in\mathcal{C}^1(D)$ in Taylor series at the point $(x_i,y)\in D_{i,j}$, we have $S(x,y)=S(x_i,y)+(x-x_i)\frac{\partial S(\xi,y)}{\partial x}, (\xi,y)\in D_{i,j}$, and hence

$$|S(x,y)-S(x_i,y)| \leq h\left\|\frac{\partial S}{\partial x}\right\|_\infty. \tag{37}$$

Similarly for the the original function $\Phi\in\mathcal{C}^4(D)$, we have

$$|\Phi(x,y)-\Phi(x_i,y)| \leq h\left\|\frac{\partial \Phi}{\partial x}\right\|_\infty. \tag{38}$$

Now using (37)-(38), it is easy to see that

$$\begin{cases}|\Phi(x,y)-S(x,y)| \leq |\Phi(x,y)-\Phi(x_i,y)|+|\Phi(x_i,y)-S(x_i,y)|\\ \qquad\qquad +|S(x_i,y)-S(x,y)|,\\ \qquad\qquad \leq h\left\|\frac{\partial \Phi}{\partial x}\right\|_\infty + h\left\|\frac{\partial S}{\partial x}\right\|_\infty+|\Phi(x_i,y)-S(x_i,y)|.\end{cases} \tag{39}$$

From [19], it is known that

$$\begin{aligned}|\Phi(x_i,y)-S(x_i,y)| \leq & h_j^* A_i(\Phi)\max_{1\leq j\leq n-1}\Big\{\Big|\frac{\partial\Phi(x_i,y_j)}{\partial y}-z_{i,j}^y\Big|,\\ & \Big|\frac{\partial\Phi(x_i,y_{j+1})}{\partial y}-z_{i,j+1}^y\Big|\Big\}+h_j^{*4}\max_{1\leq j\leq n-1}B_{i,j}(\Phi).\end{aligned} \tag{40}$$

Substituting (40) in (39), we have

$$\begin{aligned}|\Phi(x,y)-S(x,y)| \leq & h\left\|\frac{\partial \Phi}{\partial x}\right\|_\infty + h\left\|\frac{\partial S}{\partial x}\right\|_\infty + h_j^* A_i(\Phi)\max_{1\leq j\leq n-1}\Big\{\Big|\frac{\partial\Phi(x_i,y_j)}{\partial y}-z_{i,j}^y\Big|,\\ & \Big|\frac{\partial\Phi(x_i,y_{j+1})}{\partial y}-z_{i,j+1}^y\Big|\Big\}+h_j^{*4}\max_{1\leq j\leq n-1}B_{i,j}(\Phi).\end{aligned} \tag{41}$$

Since (41) is true for every $(x,y)\in D_{i,j}, i=1,2,\ldots,m-1, j=1,2,\ldots,n-1$, the uniform error bound between Φ and S is given by

$$\begin{cases}\|\Phi-S\|_\infty \leq h\left\|\frac{\partial \Phi}{\partial x}\right\|_\infty + h\left\|\frac{\partial S}{\partial x}\right\|_\infty + h^*\max\limits_{1\leq i\leq m}A_i(\Phi)\max\limits_{1\leq i\leq m}\Big[\max\limits_{1\leq j\leq n-1}\Big\{\Big|\frac{\partial\Phi(x_i,y_j)}{\partial y}\\ \qquad -z_{i,j}^y\Big|,\Big|\frac{\partial\Phi(x_i,y_{j+1})}{\partial y}-z_{i,j+1}^y\Big|\Big\}\Big]+h^{*4}\max\limits_{1\leq i\leq m}\Big\{\max\limits_{1\leq j\leq n-1}B_{i,j}(\Phi)\Big\}.\end{cases} \tag{42}$$

Using (36) and (42) together with inequality $\|\Psi-\Phi\|_\infty\leq\|\Psi-S\|_\infty+\|S-\Phi\|_\infty$, we obtain the desired estimate for $\|\Psi-\Phi\|_\infty$. □

Convergence result: For the convergence results of monotonic rational quadratic FIS Ψ, it is assumed that the estimations $U_x(\alpha)$, $U_y(\alpha^*)$, $\max\limits_{1\le i\le m} A_i(\Phi)$, $\max\limits_{1\le i\le m}\Big\{\max\limits_{1\le j\le n-1} B_{i,j}(\Phi)\Big\}$, $\max\limits_{1\le i\le m}\Big\{\max\limits_{1\le j\le n-1}\Big\{\Big|\frac{\partial\Phi(x_i,y_j)}{\partial y}-z^y_{i,j}\Big|,\Big|\frac{\partial\Phi(x_i,y_{j+1})}{\partial y}-z^y_{i,j+1}\Big|\Big\}$ are bounded as $h\to 0^+$ and $h^*\to 0^+$. Since $|\alpha|_\infty<\frac{h}{x_m-x_1}$ and $|\alpha^*|_\infty<\frac{h^*}{y_n-y_1}$, Theorem 6.1 gives that the monotonic rational quadratic FIS converges uniformly to the original function as $h\to 0^+$ and $h^*\to 0^+$.

7. Conclusion

In this study, a new type of fractal surface construction scheme is developed over a rectangular grid. The proposed interpolant not only stitch the data points arranged over the rectangular grid in a smooth fashion but also preserve the inherent shape feature, namely the monotonicity/symmetric features of the surface data. Data dependent optimal range restrictions on the scaling parameters have been developed to preserve the monotonicity feature of fractal boundary curves. One important notable thing is that the monotonic behavior of our rational quadratic FIS completely depends only on the monotonic behavior of the fractal boundary curves. The condition on the scaling matrices is developed to acquire the symmetric/non-symmetric rational quadratic FISs for given symmetric surface data. Pleasingness of graphical display and the power of the proposed fractal surface interpolant have been demonstrated through practical examples. Our method offers different shapes of monotonic rational quadratic FISs for the same surface data. An upper bound of the uniform error between the monotonic rational quadratic FIS and an original function is estimated. From this estimation, we conclude that the monotonic rational quadratic FIS has linear convergence to the original function.

Acknowledgements: The first author is thankful to the Science and Engineering Research Council, Department of Science and Technology India (Project No. SR/S4/MS: 694/10).

References

[1] S. Asaturyan and K. Unsworth, A $\mathcal{C}^1$ monotonicity preserving surface interpolation scheme, Report CS 88/02, Department of Math. and Comp. Science, University of Dundee, UK, 1988.
[2] M. R. Asim and K. W. Brodlie, Curve drawing subject to positivity and more general constraints, Computers and Graphics, 27 (2003) 469-485.
[3] M. F. Barnsley, Fractal functions and interpolation, Constr. Approx., 2 (1986) 303- 329.
[4] M. F. Barnsley and A. N. Harrington, The calculus of fractal interpolation functions, J. Approx. Theory, 57 (1989) 14-34.
[5] R. K. Beatson and Z. Ziegler, Monotonicity preserving surface interpolation, SIAM J. Numer. Anal., 22(2) (1985) 401-411.
[6] P. Bouboulis and L. Dalla, Closed Fractal Interpolation Surfaces, J. Math. Anal. Appl. 327, 116-126 (2007).
[7] R. E. Carlson and F. N. Fritsch, Monotone piecewise bicubic interpolating, SIAM J. Numer. Anal., 22(2) (1985) 386-400.
[8] G. Casciola and L. Romani, Rational interpolants with tension parameters, J. Curves and Surface Design, 2003, 41-50.
[9] A. K. B. Chand and G. P. Kapoor, Generalized cubic spline fractal interpolation functions, SIAM J. Numer. Anal., 44(2) (2006) 655-676.
[10] A. K. B. Chand and M. A. Navascués, Natural bicubic spline fractal interpolation, Nonlinear Anal., 69 (2008) 3679-3691.
[11] A. K. B. Chand and M. A. Navascués, Generalized Hermite fractal interpolation, Rev. Read. Acad. Cienc. Zaragoza, 64(2) (2009) 107-120.
[12] A. K. B. Chand, Coalescence cubic spline fractal interpolation surfaces, J. Numer. Anal. and Modeling, 3(2) (2012) 1-16.

[13] A. K. B. Chand and N. Vijender, Monotonicity preserving rational quadratic fractal interpolation functions, Adv. in Numer. Anal., 2014, 17 pages, Article Id 504825.
[14] A. K. B. Chand and P. Viswanathan, A constructive approach to cubic Hermite fractal interpolation function and its constrained aspects, BIT Numer. Math., 53 2013 841-865.
[15] B. L. Cox and J. S. Y. Wang, Fractal surfaces: measurement and applications in the earth sciences, Fractals, 1(1) (1993) 87-115.
[16] L. Dalla, Bivariate fractal interpolation on grids, Fractals, 10(1) (2002) 53-58.
[17] Z. Feng, Y. Feng, and Z. Yuan, Fractal interpolation surfaces with function vertical scaling factors, Appl. Math. Lett., 25(11) (2012) 1896-1900.
[18] J. S. Geronimo and D. P. Hardin, Fractal interpolation functions from $\mathbb{R}^n \to \mathbb{R}^m$ and their projections, Z. Anal. Anwend., 12 (1993) 535-548.
[19] J. A. Gregory, R. Delbourgo, Piecewise rational quadratic interpolation to monotonic data. IMA J. Numer. Anal. 2 (1982) 123-130.
[20] A. Kouibia and M. Pasadas, Approximation by interpolating variational splines, J. Comput. and Appl. Math., 218 (2008) 342-349.
[21] B. B. Mandelbrot, Fractals: Form, Chance and Dimension, W. H. Freeman, San Francisco, 1977.
[22] M. A. Navascués and M. V. Sebastián, Smooth fractal interpolation, J. Inequal and Appl., Article ID 78734 (2006) 1-20.
[23] S. Ogawa, P. Baveye, W. Boast, J. Y. Parlange, and T. Steenhuis, Surface fractal characteristics of preferential flow patterns in field soils : evaluation and effect of image processing, Geoderma, 88 (1999) 109-136.
[24] M. Olivier, The effect of fractal surface roughness on diffusion and reaction in porous catalysts from fundamentals to practical applications, Catalysis Today, 53 (1999) 225-243.
[25] H. Xie and H. Sun, The study of bivariate fractal interpolation functions and creation of fractal interpolated surfaces, Fractals, 5(4) (1997) 625-634.
[26] N. Zhao, Construction and application of fractal interpolation surfaces, Vis. Comput., 12 (1996) 132-146.

Department of Mathematics, Indian Institute of Technology Madras, Chennai - 600036, India, Phone: +91-44-22574629, Fax : +91-44-22574602
E-mail: chand@iitm.ac.in and vijendernallapu@gmail.com